Bulletin of the Seismological Society of America, Vol. 105, No. 3, pp. 1349–1358, June 2015, doi: 10.1785/0120140258

Ⓔ

Detecting Deep Tectonic Tremor in Taiwan with a Dense Array

by Wei-Fang Sun,* Zhigang Peng, Cheng-Horng Lin, and Kevin Chao†

Abstract We perform a systematic detection of deep tectonic tremor beneath the southern Central Range in Taiwan using a dense, small-aperture seismic array. Deployed in February 2011, the array has been recording tectonic tremor nearly continuously for 134 days, including tremor triggered by the 2011 M_w 9.0 Tohoku-Oki earthquake. We use broadband frequency–wavenumber beamforming and moving-window grid-search methods to compute array parameters for all continuous data and identify tremor as coherent nonimpulsive seismic signals with deep incidence angles. The obtained array parameters closely match with those of relocated local earthquakes and triggered tremor bursts located by the waveform envelope correlation and clustering (WECC) method, indicating the robustness of our array technique. During the 134-day study period, we detect tremor for 44 days, with a total duration of 1481 min, three to six times as long as the detection of tremor by the WECC method. We find a relative quiescence in ambient tremor activity for about 20 days following the 2011 Tohoku-Oki earthquake, suggesting that dynamic stresses from the distant mainshock triggered most tremor close to failure, resulting in a temporary lack of tremor activity. In some cases, we observe rapid tremor migration with a speed at the order of 40–50 km/hr that is similar to the speed of fast tremor migration along dip on narrow streaks in Japan and Cascadia. Our results suggest that dense array techniques are capable of capturing detailed spatiotemporal evolutions of tremor behaviors in southern Taiwan.

Online Material: Tables of station coordinates and tremor event parameters, and figures of the moving-window grid-search test with local earthquakes, tremor triggered by the 2011 Tohoku-Oki earthquake, and additional examples of detected ambient tremors.

Introduction

Deep tectonic tremor, previously named nonvolcanic tremor, has been observed at the subduction zones around the Pacific Rim (Peng and Gomberg, 2010; Beroza and Ide, 2011, and references therein). Unlike regular earthquakes, deep tremor is recognized as having nonimpulsive, low-amplitude, and long-duration signals (Obara, 2002) and often accompanies slow-slip events (Rogers and Dragert, 2003). Because most recent studies have shown that tremor activity mainly is distributed along the major fault interfaces and below the seismogenic zones where regular earthquakes occur (Shelly and Hardebeck, 2010; Ghosh *et al.*, 2012), a systematic study of tremor activity can help to better understand necessary conditions related to tremor occurrence and fault mechanics at the bottom of the seismogenic layer.

At strike-slip faults or inland faulting systems, tremor has been found along the San Andreas fault (SAF) system in California (Nadeau and Dolenc, 2005; Gomberg *et al.*, 2008; Peng *et al.*, 2009; Shelly *et al.*, 2009, 2011), the Alpine fault in the South Island of New Zealand (Wech *et al.*, 2012), the Queen Charlotte margin in western Canada (Aiken *et al.*, 2013), the Oriente fault in Cuba (Peng *et al.*, 2013), and in the Kyushu and Kanto areas in Japan (Obara and Chao, 2013). In the arc-continent collision environment in Taiwan, tremor is found mainly beneath the southern Central Range (Peng and Chao, 2008; Tang *et al.*, 2010, 2013; Chao *et al.*, 2011, 2012, 2013; Chuang *et al.*, 2014; Idehara *et al.*, 2014).

The Island of Taiwan (Fig. 1) is located at the boundary between the Eurasian and the Philippine Sea plates with two subduction systems—the Ryukyu Trench in the northeast and the Manila Trench in the southwest (Tsai, 1986; Angelier *et al.*, 2001), with convergent rates of 5 cm/yr^{-1} (Nishizawa *et al.*, 2009) and 2–10 cm/yr^{-1} (Galgana *et al.*, 2007), respectively. Between the north-dipping subduction zone to the northeast and the east-dipping subduction zone to the southwest of the island, the Luzon volcanic collides into the

*Now at Department of Natural Resources and Environmental Studies, National Dong Hwa University, 1, Sec. 2, Da Hsueh Road, Shoufeng, Hualien 97401, Taiwan.

†Now at Department of Earth, Atmospheric and Planetary Sciences, Massachusetts Institute of Technology, 77 Massachusetts Avenue, Cambridge, Massachusetts 02139-4307.

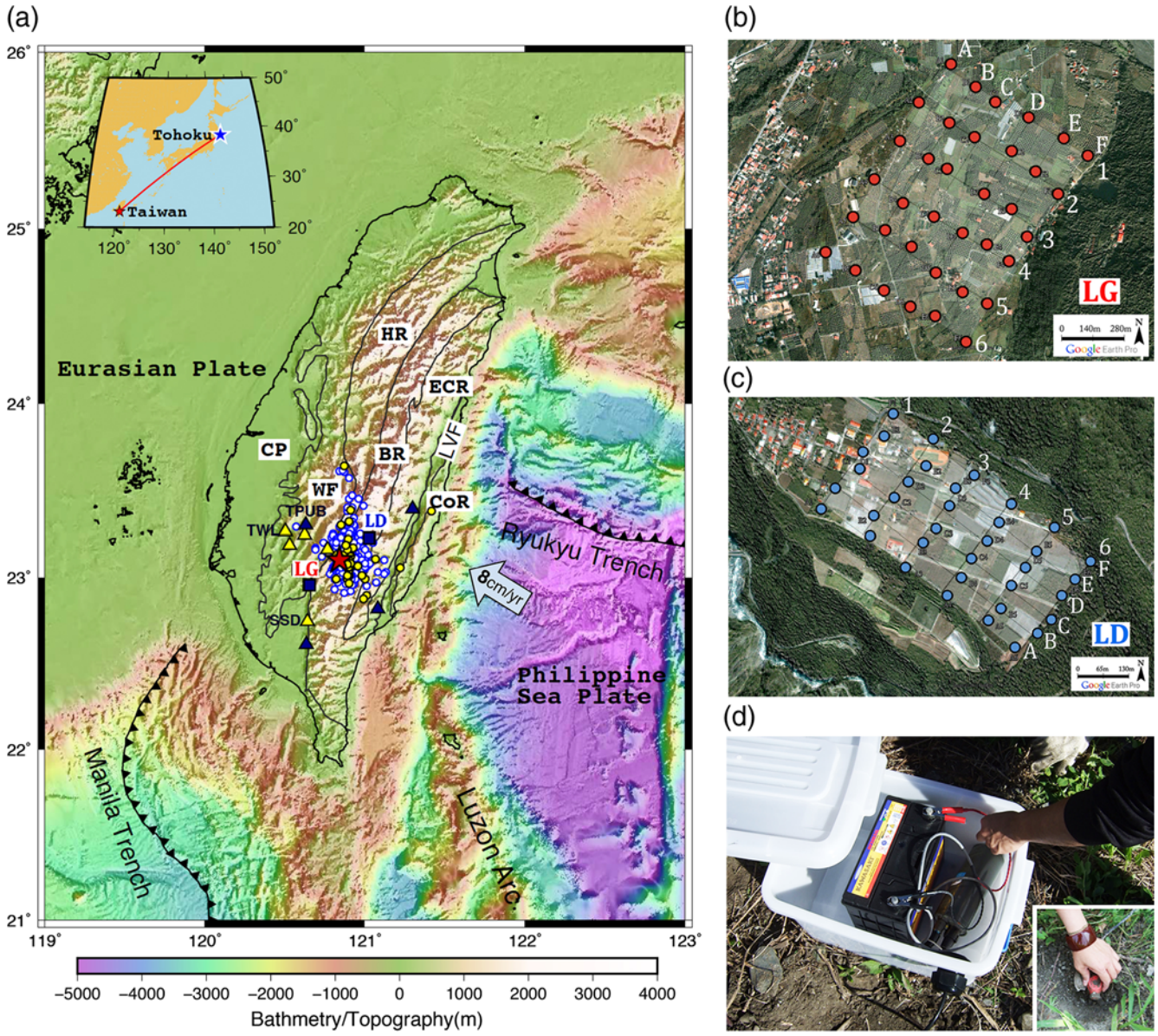

Figure 1. Map of study region in Taiwan and detailed instrument deployment plan. (a) The average-triggered tremor source following the 2011 M_w 9.0 Tohoku-Oki mainshock (Chao *et al.*, 2013) is marked as the solid star. The squares indicate the locations of the Liouguei (LG) and the Lidao (LD) arrays. The solid and open circles are ambient tremor sources detected by Chao *et al.* (2011) and Chuang *et al.* (2014), respectively. The dark and gray triangles are the adjacent, permanent Broadband Array in Taiwan for Seismology (BATS) and Central Weather Bureau Seismic Network (CWBSN) stations, respectively. Geological provinces: CP, Coastal plain; WF, Western foothill; HR, Hsueshan Range; BR, Backbone Range or Tananao schist complex; ECR, East Central Range; LVF, Longitudinal Valley fault; and CoR, Coastal Range. The arrow indicates the convergent direction of two plates (Yu *et al.*, 1997). The inset shows the ray path of the 2011 Tohoku-Oki mainshock. (b) The configuration and station locations (circles) of the LG array in a grid of 140 × 180 m. (c) The configuration and station locations (circles) of the LD array in a grid of 65 × 130 m. (d) Instrument setting: the TEXAN data logger connects to a car battery in the box, and the inset shows the vertical-channel GS-11D sensor (geophone) with a 4.5 Hz natural frequency. The color version of this figure is available only in the electronic edition.

Chinese continental margin with a convergence rate of about 8 cm/yr^{-1} (Yu *et al.*, 1997). Such a collision creates the Central Range (HR, BR, and ECR in Fig. 1), the backbone of the island.

Peng and Chao (2008) first identified triggered tremor beneath the Central Range following the 2001 M_w 7.9 Kunlun earthquake in northern Tibet. Subsequent tremor studies mainly focus on low-frequency earthquakes (Tang *et al.*, 2010, 2013) and both triggered (Chao *et al.*, 2012, 2013) and ambient tremor (Chao *et al.*, 2011; Chuang *et al.*, 2014; Idehara *et al.*, 2014) in the southern Central Range. Those studies utilized seismic data from two permanent seismic networks—the Broadband Array in Taiwan for Seismology (BATS) operated by the Institute of Earth Sciences in Academia Sinica (Kao *et al.*, 1998) and the short-period Central Weather Bureau Seismic Network (CWBSN) and the Broadband Seismic Network

operated by the Central Weather Bureau (CWB) (Shin *et al.*, 2013)—and one temporarily deployed linear array, the Taiwan Integrated GEodynamic Research (TAIGER) (Huang *et al.*, 2013; Wu *et al.*, 2014). The spatiotemporal distribution of tremor has been mapped (Chao *et al.*, 2011; Chuang *et al.*, 2014) using the waveform envelope correlation and clustering (WECC) method (Wech and Creager, 2008; Wech, 2010). However, due to relatively sparse station distribution of the BATS and CWB networks near the tremor source region and elevated background noises on the Island of Taiwan, obtaining a complete list of tremor activity is difficult.

High-quality seismic data recorded by dense small-aperture seismic arrays have been used to increase tremor detectability and to obtain high-resolution tremor location in Cascadia (La Rocca *et al.*, 2008; Ghosh *et al.*, 2009, 2010, 2012) and the SAF (Fletcher and Baker, 2010; Ryberg *et al.*, 2010; Ghosh, 2014). In Cascadia, when the multibeam-back-projection method is applied to the array data (Ghosh *et al.*, 2012), nearly continuous tremor activities were detected. The array-based results provide detailed spatiotemporal evolutions of tremor activities when compared with the network-based methods, such as the WECC method (e.g., Wech and Creager, 2008), the source-scanning algorithm (Kao *et al.*, 2006), and the waveform-matching technique (Shelly *et al.*, 2007a).

To better understand tremor behaviors in the southern Central Range, we installed two temporary dense seismic arrays in 2011. This deployment was fortunate, because it captured triggered tremor following the 11 March 2011 M_w 9.0 Tohoku-Oki earthquake (Chao *et al.*, 2013) and many background tremor episodes. In this study, we combine the broadband frequency–wavenumber (BBFK) beamforming (Nawab *et al.*, 1985; Goldstein *et al.*, 2003) and the moving-window grid-search (MWGS) (Frankel *et al.*, 1991; Fletcher *et al.*, 2006; Fletcher and Baker, 2010) methods to detect weak tremor signals. We also use triggered tremor bursts and local earthquakes to test the detection ability of each array. In addition, we compare our detection results with other tremor catalogs using the WECC technique (Chao *et al.*, 2011; Chuang *et al.*, 2014) and discuss the implications of these findings.

Data and Analysis Procedure

In 2011, we installed two dense small-aperture seismic arrays in the Liouguei (LG array) and the Lidao (LD array) areas at the southwest and northeast sides of the tremor source region, respectively (Fig. 1). Each array includes 36 short-period vertical-channel GS-11D sensors with 4.5 Hz natural frequency. We recorded continuous ground-velocity data at 100 samples/s. The instruments were deployed in areas of 700 m × 900 m for the LG array (Fig. 1b; Ⓔ Table S1, available in electronic supplement to this article) and 300 m × 650 m for the LD array (Fig. 1c; Ⓔ Table S2) on a relatively flat part of each mountain area. We used the TEXAN data loggers to record seismic data. The original design of these loggers contains two D alkaline batteries, which can only last for about 5–7 days of continuous recording. We used an external wire designed for TEXAN to connect to a 12V/45Ah car battery so that the TEXAN could record continuously for about 20–22 days before battery replacement (Fig. 1d). Data for some stations are available from 1 January 2011. However, the recording is mostly complete for a total of 134 days from 12 February 2011 to 7 July 2011 (Julian days 43–188). During this time, we did not have recordings for 12 days (2011 Julian days 62, 63, 84, 85, 105, 106, 126, 127, 147, 148, 168, and 169) due to instrument repair and battery replacement about every 20 days.

In this study, we detected tremor by two array-processing techniques, the BBFK beamforming (Nawab *et al.*, 1985; Goldstein *et al.*, 2003) and the MWGS (Frankel *et al.*, 1991; Fletcher *et al.*, 2006; Fletcher and Baker, 2010) methods. Both methods have a plane-wave assumption so that the differential travel time of the plane-wave front is due to a specific slowness and back azimuth. We corrected for such time shifts with the best-fitting slowness and back azimuth then stacked all signals (i.e., delay and sum) to obtain an array-averaged recording (Rost and Thomas, 2002; Fletcher *et al.*, 2006; Ghosh *et al.*, 2009).

For the BBFK method, the peak frequency–wavenumber (f-k) of the dominant signals is calculated in the frequency domain. The wavenumber k (1/km) of the plane wave is calculated by the equation $k = f \times p$, in which f (Hz) is frequency and p (s/km) is horizontal slowness. The wavenumber and slowness were obtained from the maximum amplitude of the wavenumber spectrum (Helffrich *et al.*, 2013). We used the built-in command of BBFK in the Seismic Analysis Code (SAC) to compute BBFK spectra (Nawab *et al.*, 1985; Goldstein *et al.*, 2003).

For the MWGS method, the peak cross-correlation coefficient (CC) values of time-corrected waveforms due to slowness vectors are calculated in the time domain (Fletcher *et al.*, 2006). We developed a MATLAB-based technique (see Data and Resources) with the following steps. First, we calculated the time correction as a function of slowness of seismograms for all stations in both arrays. Next, we obtained the CC values as a function of slowness by averaging correlation functions of all the individual station pairs. The peak CC value corresponds to the best-fitting azimuth and apparent velocity for signals in a specific time window (Fletcher *et al.*, 2006).

The detailed analysis procedure is given below. We first filtered the seismic data in the 5–20 Hz frequency range. This range is slightly higher than the typical 1–10 Hz frequency range for tremor studies (Obara, 2002). We chose 5–20 Hz mainly because the instrument corner frequency is 4.5 Hz. In addition, the tight array allows us to include higher frequencies in this study. Finally, the 2011 Tohoku-Oki mainshock and its intensive aftershock sequences were capable of producing P-wave signals up to 5 Hz (Ⓔ Fig. S1). Hence, if we filtered the data in the nominal tremor band of 1–10 Hz, it would contaminate the results. On the other hand, locally triggered or ambient tremor can generate signals above the background noises up to 20 Hz (Figs. 2 and 3).

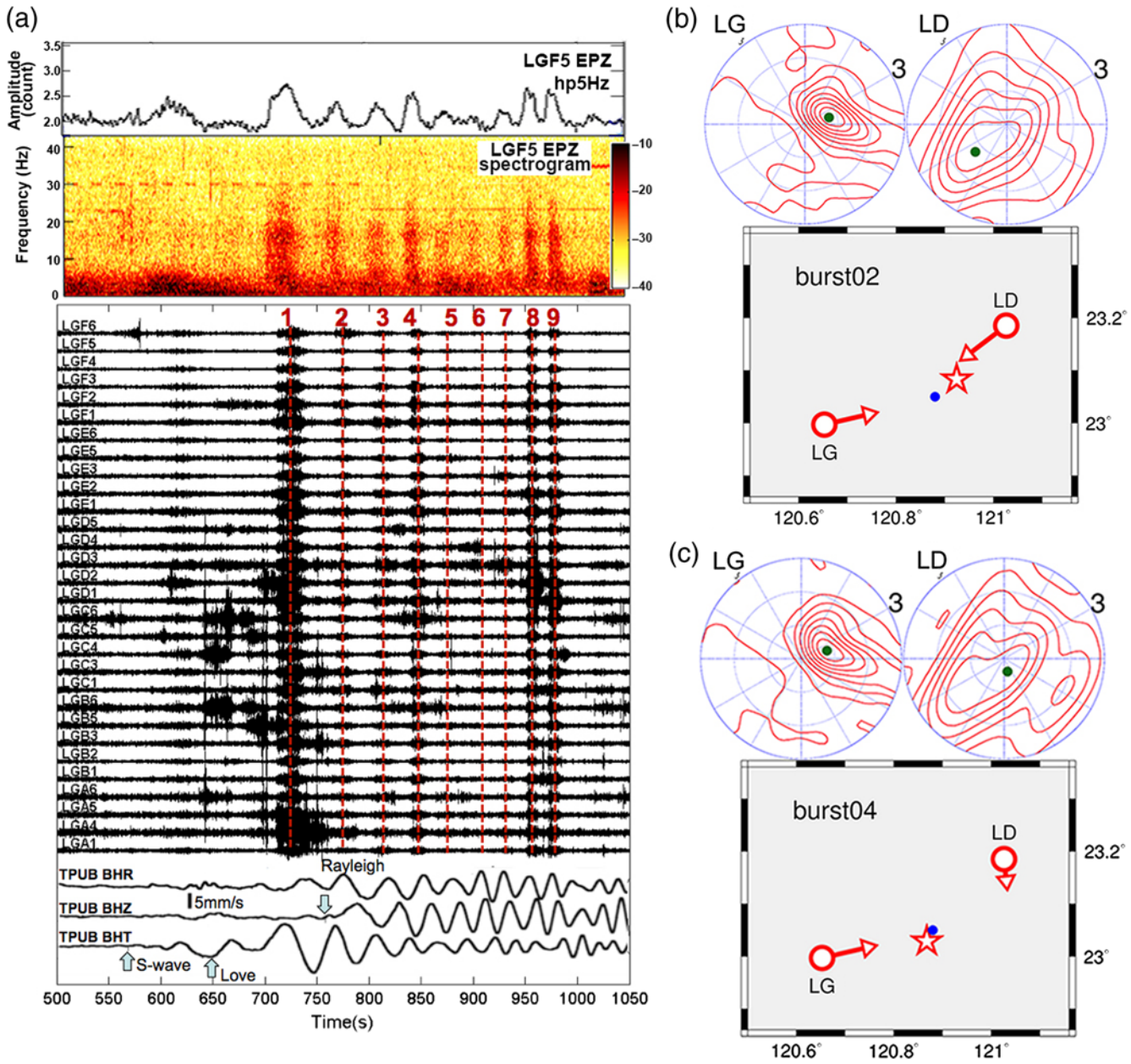

Figure 2. The deep tremor triggered by the 2011 M_w 9.0 Tohoku-Oki earthquake recorded at the LG array and the broadband frequency–wavenumber (BBFK) results for the nine tremor bursts. (a) (Top) The $\log_{10}$ 5-Hz high-pass envelope function, (middle) spectrogram, and (bottom) the 5–20 Hz band-pass-filtered seismograms recorded the nine tremor bursts triggered by the 2011 Tohoku-Oki mainshock. (b) and (c) The BBFK detections are shown for burst 2 and 4, respectively. (Top) The contour plots denote the distribution of frequency–wavenumber (f-k) amplitude (beam power) as a function of back azimuth (angle) and wavenumber (radius), and the location of the f-k peak (dot) marks the best solution of back azimuth and wavenumber. (Bottom) The circles indicate the locations of the LG and the LD arrays, and the direction and length of each arrow represent the back azimuth and the wavenumber, respectively. The star and the dot are the locations of each tremor burst and the average tremor source, respectively, determined by the conventional envelope cross-correlation method (Chao *et al.*, 2013). The color version of this figure is available only in the electronic edition.

We used BBFK in SAC to compute BBFK spectra and then obtained the best-fitting back azimuth and wavenumber for every 2-min time window with a 50% overlapping (i.e., 1-min shift each time), the same time window setting as in Ghosh *et al.* (2010). For the MWGS method, we used the 20 s nonoverlapping sliding window and searched for the best-fitting back azimuth and apparent velocity with the maximum CC value. Here, a smaller window size is used to follow the time window setting in Fletcher and Baker (2010).

Next, we combined the parameters obtained by BBFK and MWGS and band-pass-filtered envelope functions to visually identify tremor events. The criteria for eligible tremor detections are (1) the detected duration time is longer than 3 min, and the array envelope function is coherent among

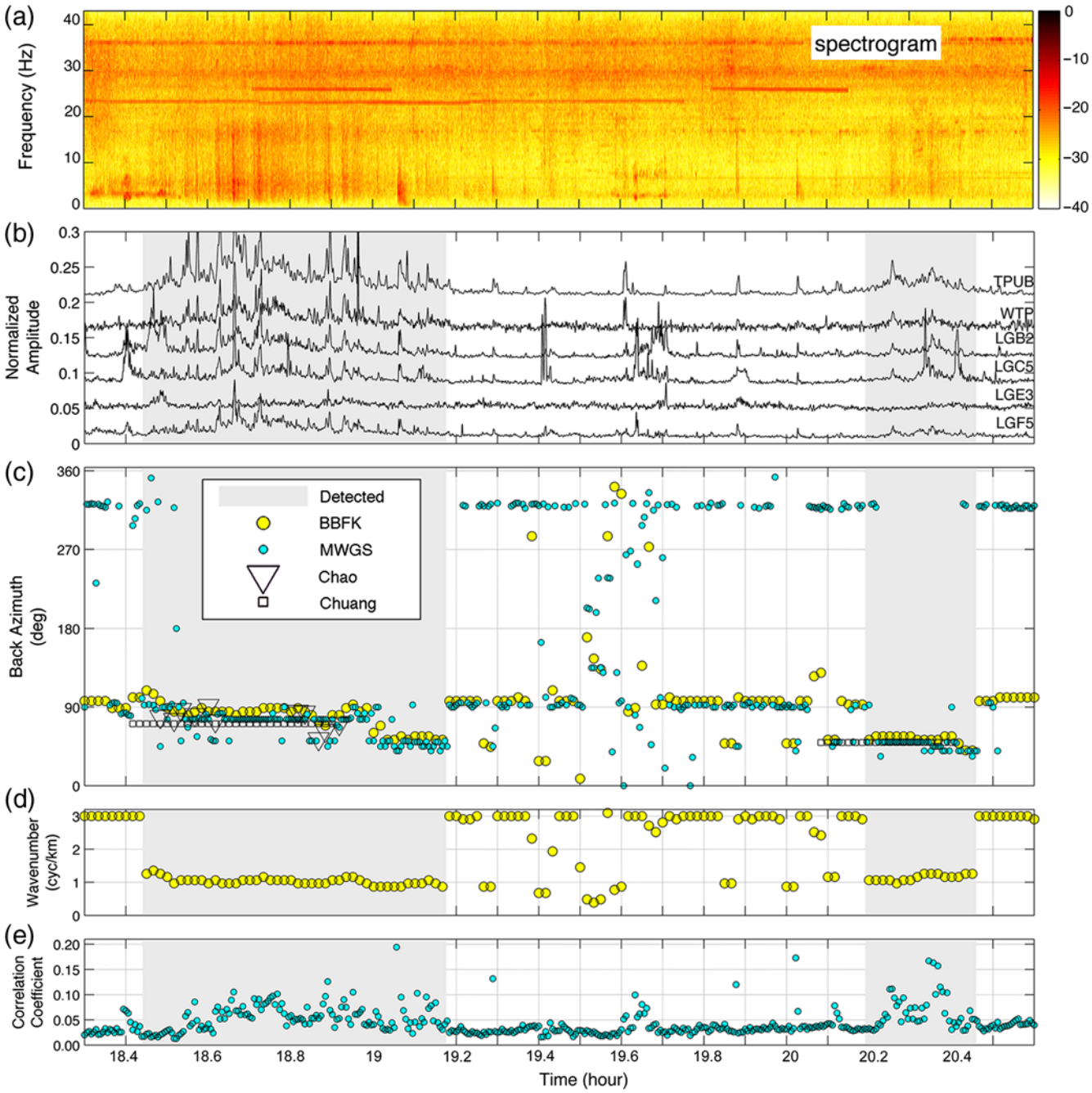

Figure 3. An example of ambient tremor detected by three methods. (a–e) The spectrogram, normalized envelope function, back azimuth, wavenumber, and correlation coefficient versus UTC time on 2011 Julian day 151. The shaded areas mark the tremor period identified by the combined BBFK–MWGS (moving-window grid-search) method and visual inspection. Other symbols and notations are marked in the legend. The color version of this figure is available only in the electronic edition.

nearby permanent and temporary seismic stations in each array (Fig. 1); (2) the back azimuth obtained by both methods is consistent within 30° due to the relative position between the arrays and tremor sources (Fig. 1); (3) the wavenumber obtained from BBFK is $\lesssim$1.5 (cycle/km), which implies the seismic energy has a steep incidence angle; and (4) the waveform CC values observed from MWGS is $\gtrsim$0.02. The choices of these parameters are empirical, but with a common goal to detect tremor signals with stable azimuth and deep origin. In addition, we removed the detections of local and distant earthquakes by comparing our results with the local CWB and the global Advanced National Seismic System (ANSS) earthquake catalogs.

Robustness Test with Local Earthquakes and Triggered Tremor

To evaluate the robustness of our methods, we selected 111 nearby local earthquakes to test the detection ability by

using the MWGS method with some adjustment in the parameters suitable for detecting earthquakes. Those relocated earthquakes (Wu *et al.*, 2008) are one month before and after the 2011 M_w 9.0 Tohoku-Oki mainshock, with local magnitude (M_L) between 1.0 and 3.9 and epicenter distances less than 53 km to each array. Specifically, we manually picked the *S* arrival and used a 0.3–0.4 s time window to include the first few cycles of the *S* wave of each earthquake to obtain the MWGS parameters. According to the back-azimuth differences between the relocated catalogs (Wu *et al.*, 2008) and obtained back azimuths by MWGS among the 111 local earthquakes, the LG array provides more accurate detections, with 104 of them (94%) $<20°$. In comparison, 94 back-azimuth solutions (85%) had errors $>20°$ for the LD array. A detailed examination of waveforms recorded at the LD array also revealed possible time shifts at some stations (e.g., LDA6, LDC6, LDD6, and LDF6) after accounting for the slowness and incidence angle.

We also applied both the BBFK and MWGS methods to detect triggered tremor following the 2011 Tohoku-Oki earthquake. Both the LG (Fig. 2a) and the LD (Ⓔ Fig. S2) arrays recorded nine clear, triggered tremor bursts during the passing surface waves of the 2011 Tohoku-Oki mainshock. As shown in Figure 2 (and also Ⓔ Fig. S4 and Ⓔ Table S3), the back azimuths obtained by the BBFK with only the LG array match well with the burst locations from the conventional envelope cross-correlation method (Chao *et al.*, 2013).

These comparisons indicate that our array technique is robust and can be used to detect tremor episodes in Taiwan, but there were some timing issues at the LD array. Because the TEXANs were connected to the Global Positioning System (GPS) for synchronization only before and after each three-week acquisition, it is possible that the observed time shifts could be due to timing errors in the TEXANs. We checked the time drifts for all stations (Ⓔ Fig. S3) and found that drift values during the acquisitions were extremely small ($<1\times10^{-7}$ s). Hence, we concluded that TEXAN timing was not the primary cause. We noticed that stations (LDA6, LDC6, LDD6, and LDF6) showing the most discrepancies with the predicted arrivals were all close to the edge of the LD array and the flat land (Fig. 1c). Hence, it is possible that lack of consistencies between the predicted and observed back azimuths (for regular earthquakes) could be partially due to complicated local site conditions at the LD array. Because of this, in the following sections, we only present results by applying both techniques to the LG array.

Ambient Tremor Detection

Figure 3 shows an example of ambient tremor detected on 31 May 2011. Between 18:27 and 19:10 UTC, we observed a clear reduction in the wavenumber, indicating the seismic signals have steep incidence angles during this time period. In the meantime, the back azimuths measured from both the BBFK and MWGS methods are stable, with mean values of 83° and 71°, respectively. The coherent tremor signals were also recorded by nearby BATS station TPUB and CWBSN station WTP (Fig. 3b). Finally, this tremor episode was also detected by other recent studies (Chao *et al.*, 2011; Chuang *et al.*, 2014), and the obtained back azimuths are comparable. Ⓔ Figure S5 shows an example of ambient tremor events only detected by this study. The tremor episodes not detected by the other two catalogs were generally weaker with shorter durations, which would partially explain why they were not detected by the standard WECC method (Fig. 4).

Radiated seismic energy of an earthquake can be computed by integrating radiated energy flux in velocity-squared seismograms (Boatwright and Choy, 1986). To compare equivalent radiated seismic energy among triggered and ambient tremor, we simply sum the square of instrument-corrected velocity after high-pass filtering by 5 Hz within individual tremor windows recorded by the BATS station TPUB. We then normalize it by the value of triggered tremor following the 2011 Tohoku-Oki mainshock. We use such normalization to remove the potential distance/attenuation effect (by assuming that triggered tremor originated from the same places of ambient tremor) and to compare the radiated energy between triggered and ambient tremor. Figure 4a shows the normalized equivalent radiated energy (NERE) of triggered tremor is 1–3 orders greater than that of ambient tremor. In addition, it appears that our method can detect tremor with weaker-radiated energy than that detected by the other two WECC methods. After dividing the NERE by duration of individual tremor episodes, we obtain the NERE rate. As shown in Figure 4b,c, tremor detected only by our method is generally shorter in duration and weaker in NERE rate and amplitude.

In total, we identified 44 days containing at least one tremor episode among the 134-day period (Fig. 5). The total duration is 1481 min, and the average duration is 17 min (Ⓔ Table S4). The total tremor duration detected by our array method is 6 times more than that detected by Chao *et al.* (2011) (27 days/239 min) and 3 times more than that detected by Chuang *et al.* (2014) (21 days/450 min). Overall, the tremor detected by the BBFK and MWGS methods is similar to the other two catalogs in time, except that our catalog shows nearly continuous tremor activities after Julian day 176 (Fig. 5). Interestingly, there was no tremor activity reported by three different studies (Chao *et al.*, 2011; Chuang *et al.*, 2014; and this study) in the 10-day period following the 2011 M_w 9.0 Tohoku-Oki earthquake, and the tremor rate returned back to previous recurrence cycle after 20 days (Figs. 4 and 5). We also applied a 2–8 Hz filter to all the data and repeated the analysis. The obtained temporal evolutions are similar to those from 5–20 Hz filtered data (Fig. 5).

Ⓔ Figure S6 shows a summary of back azimuths and wavenumbers for tremor detections and all time windows analyzed by the BBFK method. Because the LG array was located at the southwestern side of the tremor source regions, the ranges of back azimuths for all observed tremor are from N 45° to N90°E (Ⓔ Fig. S6a). The tremor signal is barely visible throughout the entire set of time windows, and the

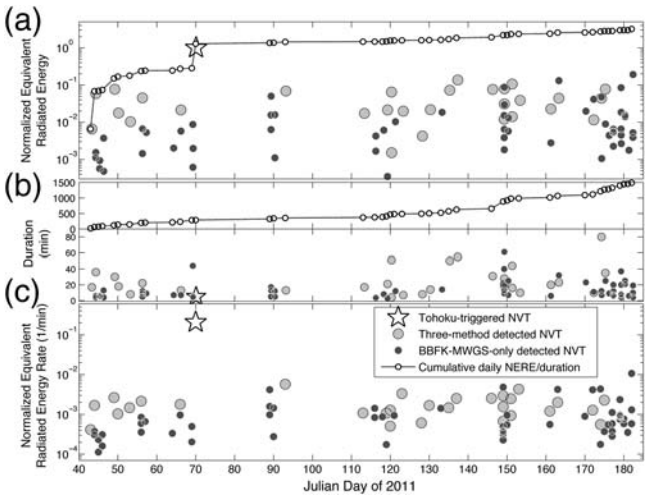

Figure 4. Normalized equivalent-radiated energy (NERE) and duration of detected tremor from three methods. The open stars denote the triggered tremor following the surface waves of the 2011 Tohoku-Oki earthquake; the light and the dark gray dots indicate ambient tremor detected by both the waveform envelope correlation and clustering (WECC) and our BBFK–MWGS methods and by only our BBFK–MWGS method, respectively. (a) NERE of individual tremor episodes and cumulative, daily, radiated energy (circles and dashed line). (b) Duration of individual tremor episodes and cumulative daily duration (circles and dashed line). (c) NERE rate.

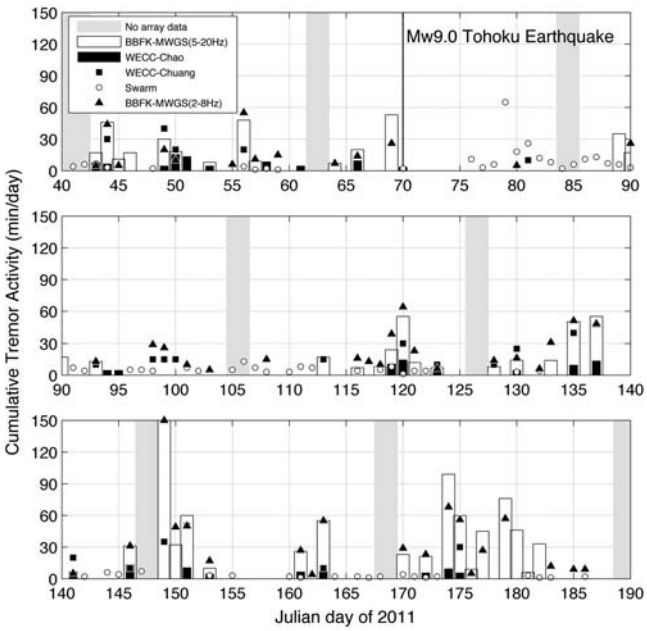

Figure 5. Daily tremor activity obtained in three studies: combined BBFK–MWGS from this study (open histograms are for 5–20 Hz and solid triangles for 2–8 Hz), WECC-Chao by Chao *et al.* (2011) (solid histograms), and WECC-Chuang by Chuang *et al.* (2014) (solid squares). The open circles indicate daily accumulative swarm activity in the adjacent area (Wei Peng, personal comm., 2014). The gray areas mark those days without array data, and the dashed line marks the occurrence time of the 2011 M_w 9.0 Tohoku-Oki earthquake.

majority of seismic sources come from between N60°E (060°) to S (180°) (Ⓔ Fig. S6b) with wavenumber equal to 3 cycles/km. Because of their shallow incidence angles, the likely sources are either shallow earthquakes from the eastern Longitudinal Valley fault (LVF in Fig. 1) or background noises from the east coast.

Among those 86 detected tremor events, some of them show migration behavior and the directions can be either southward or northward. For example, tremor sources showing in Figure 3 were concentrated in areas with back azimuths of ~85° between 18:36 and 19:00 UTC and then moved northward to a new area with back azimuths of ~55° between 19:00 and 19:10 UTC. Because we could not obtain the absolute location of the tremor source by using a single array, we used the tremor locations determined by Chao *et al.* (2011) to estimate the migration speed. A total of eight tremor events, which are both detected by Chao *et al.* (2011) and this study, show possible migration behaviors (Ⓔ Table S5). The average migration speed is ~110 km/hr (2722 km/day), similar to that observed in other regions (Ghosh *et al.*, 2009; Fletcher and Baker, 2010).

Discussion and Conclusions

In this study, we conducted a systematic detection of ambient tremor in southern Taiwan based on a temporarily deployed seismic array. The obtained tremor durations are 3–6 times greater than those detected based on permanent stations (Chao *et al.*, 2011; Chuang *et al.*, 2014). This is consistent with similar findings in Cascadia (Ghosh *et al.*, 2009, 2010, 2012), suggesting that array techniques have higher detection capabilities than traditional WECC techniques (Wech and Creager, 2008). Unfortunately, we did not have an existing fault interface model in this region (Chao *et al.*, 2012), so we were unable to project the best slowness of tremor detection back to the source region to determine the tremor location, as was done in Cascadia and other regions (e.g., Ghosh *et al.*, 2009).

The dense array also recorded nine tremor bursts (~300 s in total duration, each 20–30 s) triggered by surface waves of the 2011 Tohoku-Oki earthquake. In comparison, the durations of individual ambient tremor events vary from 3–5 min to over an hour, although their NERE rates are 1–3 orders smaller (Fig. 4c). In addition, we found an apparent lack of tremor activity for about 20 days following the 2011 Tohoku-Oki mainshock (Figs. 4 and 5). One possible source of contamination is the early aftershocks of the teleseismic mainshock, which could prevent identification and location of some triggered tremor, such as those observed at Parkfield following the 2006 M_w 8.3 Kuril Island earthquake (Peng *et al.*, 2009). However, in our case, we applied a 5–20 Hz filter prior to the array analysis, which should remove most of the teleseismic *P*-wave signals from the aftershock regions of the 2011 Tohoku-Oki mainshock (Ⓔ Fig. S1). In other words, if tremor did occur in the first 20 days following the 2011 Tohoku-Oki mainshock, it would likely have been detected by either of the WECC techniques. Hence, we argue that the lack of tremor detections following the 2011 Tohoku-Oki event is likely real. Similar quiescence of tremor

was also observed at the Parkfield–Cholame section of the SAF following large distant earthquakes (Peng *et al.*, 2009). We hypothesize the strong teleseismic event triggered most fault patches that are close to failure (i.e., time advance), resulting in a temporary lack of seismic events following the large distant events (i.e., dynamic stress shadow). Interestingly, Pollitz *et al.* (2014) observed a global quiescence of magnitude >5.5 earthquake, following a short-term global increase of magnitude >5.5 earthquakes after the 11 April 2012 M_w 8.6 Indian Ocean earthquake (Pollitz *et al.*, 2012). Yao *et al.* (2015) also found a similar seismic quiescence in south-central Tibet following a sharp increase of local seismicity that was dynamically triggered by the 2004 M_w 9.1 Sumatra earthquake and is consistent with this interpretation.

On the other hand, both Chao *et al.* (2011) and Chuang *et al.* (2014) observed that after the 4 March 2010 M_L 6.4 Jiashian earthquake, located at almost the same location as the LG array, the activities of shallow earthquake swarms (at <20 km depth) and deep tremor (at 17–34 km depth) increased for about 80 days. Similar increases of tremor activities were found at the Parkfield–Cholame section of the SAF following the 2004 M_w 6.0 Parkfield earthquake (Nadeau and Guilhem, 2009; Shelly, 2010). In these cases, the moderate earthquakes were very close (i.e., <50 km) and hence could change the overall loading rates in the tremor source region, either by static or quasi-static stress changes. Hence, the mechanism of tremor rate change may not be the same as the remotely triggered case in this study.

Several studies have found that systematic migration of ambient tremor, especially in southwest Japan and Cascadia, is common but has different migration speeds. Large-scale tremor migrates along the subduction-zone strike at about 10 km/day, which tracks the rupture front of slow-slip events (e.g., Obara, 2002; Bartlow *et al.*, 2011). Sometimes tremor propagates in the opposite direction to the prevailing tremor propagation at speeds of ~100 km/day (e.g., Houston *et al.*, 2011). Ghosh *et al.* (2012) proposed that asperities at the transition zone, located between the upper locked/seismogenic zone and the lower creeping zone, control tremor generation and rupture propagation, which makes the migration velocity slower inside the asperities and faster in between due to variation in slow-slip velocity along the subduction-zone strike. The average migration speed of some tremor events in this study, on the order of ~100 km/hour, is similar to fast tremor migration speed along dip on narrow streaks in Japan and Cascadia (e.g., Shelly *et al.*, 2007a; Ghosh *et al.*, 2010, 2012), and both ambient and triggered tremor migration at the Parkfield–Cholame section of the SAF (Shelly, 2010; Shelly *et al.*, 2011). Shelly *et al.* (2007b) propose the fast migration speed would be unlikely to accompany fluid flow but could be due to fast propagation of slow-slip events. Based on the apparent speed of propagation and the duration of tremor, we estimate that in some cases tremor would propagate up to 50 km. Assuming a similar tremor duration and moment magnitude in Cascadia, the corresponding geodetic moment would be about 4–4.5, which is well below the sensitivity of the GPS and borehole strain meters deployed at the Central Range (Ya-Ju Hsu, personal comm., 2014).

Our study demonstrates that dense array observation is effective to detect deep tectonic tremor in Taiwan. Therefore, if we can simultaneously install multiple arrays with valid station coverage around tremor sources, such as the Array of Arrays in Cascadia (Ghosh, 2011), we expect to not only detect more tremor activity, but also obtain more accurate tremor locations, especially their depths. Combining with locations of low-frequency earthquakes (e.g., Tang *et al.*, 2013; Aguiar *et al.*, 2014), earthquake swarms (e.g., Wei Peng, personal comm., 2014), and focal mechanisms of both triggered and ambient tremors, we can better understand the fault motions for generating tremor signals beneath the southern Central Range. Moreover, with the detailed spatiotemporal evolution of tremor, we can reveal the relationship between the regular earthquakes and tremor at the continental collision environment in southern Taiwan.

Data and Resources

The broadband seismic data at station TW.TPUB belongs to the Broadband Array in Taiwan for Seismology (BATS) network and is managed by Institute of Earth Sciences (IES) in Academia Sinica. The seismic data can be downloaded from the Incorporated Research Institutions for Seismology Data Management Center (IRIS DMC) website, http://www.iris.edu/mda/TW/TPUB; last accessed March 2015). The dense array was deployed by IES, and the data can be requested by contacting Cheng-Horng Lin at lin@earth.sinica.edu.tw. The broadband frequency–wavenumber (BBFK) beamforming method is from a built-in Seismic Analysis Code (SAC) command BBFK. We follow the equations in Fletcher *et al.* (2006) to write our own moving-window grid-search method. MATLAB is available at http://www.mathworks.com/products/matlab/ (last accessed April 2015).

Acknowledgments

We thank the Central Weather Bureau and the Institute of Earth Sciences in Academia Sinica, Taiwan, for providing seismic data. We also thank Yih-Min Wu for the relocated earthquake catalog, Lindsay Yu-Ling Chuang for the tremor catalog, and Wei Peng for the earthquake swarm catalog. This manuscript benefitted from useful comments by Andrew Newman and Chris Huber. W.-F. Sun is supported by a government scholarship from the Ministry of Education of Taiwan. Z. Peng is supported by a National Science Foundation (NSF) CAREER award (EAR-095605). K. Chao is supported by the Japan Society for the Promotion of Science (JSPS) through Awards P12329 and KAKENHI 23244091. This research was also supported by the Taiwan Earthquake Research Center (TEC). The TEC Contribution Number for this article is 00113.

References

Aguiar, A., K. Chao, and G. Beroza (2014). Comparing low-frequency earthquakes during triggered and ambient tremor in Taiwan, *presented at 2014 Fall Meeting, AGU*, San Francisco, California, 15–19 December, Abstract S51E-06.

Aiken, C., Z. Peng, and K. Chao (2013). Tremors along the Queen Charlotte margin triggered by large teleseismic earthquakes, *Geophys. Res. Lett.* **40,** 829–834, doi: 10.1002/grl.50220.

Angelier, J., J.-C. Lee, H.-T. Chu, J.-C. Hu, C.-Y. Lu, Y.-C. Chan, T.-J. Lin, Y. Font, B. Deffontaines, and Y.-B. Tsai (2001). Le séisme de Chichi (1999) et sa place dans l'orogène de Taiwan, *C. R. Acad. Sci. Paris, IIa* **333,** no. 1, 5–21 (in French).

Bartlow, N. M., S. Miyazaki, A. M. Bradly, and P. Segall (2011). Space-time correlation of slip and tremor during the 2009 Cascadia slow slip event, *Geophys. Res. Lett.* **38,** L18309, doi: 10.1029/2011GL048714.

Beroza, G. C., and S. Ide (2011). Slow earthquakes and nonvolcanic tremor, *Annu. Rev. Earth Planet. Sci.* **39,** 271–296, doi: 10.1146/annurev-earth-040809-152531.

Boatwright, J., and G. Choy (1986). Teleseismic estimates of the energy radiated by shallow earthquakes, *J. Geophys. Res.* **91,** no. B2, 2095–2112, doi: 10.1029/JB091iB02p02095.

Chao, K., Z. Peng, H. Gonzalez-Huizar, C. Aiken, B. Enescu, H. Kao, A. A. Velasco, K. Obara, and T. Matsuzawa (2013). A global search for triggered tremor following the 2011 M_w 9.0 Tohoku earthquake, *Bull. Seismol. Soc. Am.* **103,** no. 2B, 1551–1571, doi: 10.1785/0120120171.

Chao, K., Z. Peng, A. Wech, C.-C. Tang, C.-H. Lin, and C.-H. Chen (2011). Deep tremor activities beneath the Central Range in Taiwan and their relationship to local, regional, and teleseismic earthquakes, *Seismol. Res. Lett.* **82,** 326.

Chao, K., Z. Peng, C. Wu, C.-C. Tang, and C.-H. Lin (2012). Remote triggering of non-volcanic tremor around Taiwan, *Geophys. J. Int.* **188,** no. 1, 301–324, doi: 10.1111/j.1365-246X.2011.05261.x.

Chuang, L. Y., K. H. Chen, A. G. Wech, T. Byrne, and W. Peng (2014). Ambient tremors in a collisional orogenic belt, *Geophys. Res. Lett.* **41,** no. 5, 1485–1491, doi: 10.1002/2014GL059476.

Fletcher, J. B., and L. M. Baker (2010). Analysis of nonvolcanic tremor on the San Andreas fault near Parkfield, CA using U. S. Geological Survey Parkfield Seismic Array, *J. Geophys. Res.* **115,** no. B10, doi: 10.1029/2010JB007511.

Fletcher, J. B., P. Spudich, and L. M. Baker (2006). Rupture propagation of the 2004 Parkfield, California, earthquake from observations at the UPSAR, *Bull. Seismol. Soc. Am.* **96,** no. 4B, S129–S142, doi: 10.1785/0120050812.

Frankel, A., S. Hough, P. Friberg, and R. Busby (1991). Observations of Loma Prieta aftershocks from a dense array in Sunnyvale, California, *Bull. Seismol. Soc. Am.* **81,** no. 5, 1900–1922.

Galgana, G., M. Hamburger, R. McCaffrey, E. Corpyz, and Q. Chen (2007). Analysis of crustal deformation in Luzon, Philippines using geodetic observations and earthquake focal mechanisms, *Tectonophysics* **432,** 63–87, doi: 10.1016/j.tecto.2006.12.001.

Ghosh, A. (2011). Imaging slow earthquakes in Cascadia using seismic arrays, *Ph.D. Dissertation*, Department of Earth and Space Sciences, University of Washington, Seattle, Washington, 61–63.

Ghosh, A. (2014). Imaging tremor dynamics on SAF near Parkfield using a mini seismic array, *Seismol. Res. Lett.* **85,** no. 2, 428.

Ghosh, A., J. E. Vidale, and K. C. Creager (2012). Tremor asperities in the transition zone control evolution of slow earthquakes, *J. Geophys. Res.* **117,** B10301, doi: 10.1029/2012JB009249.

Ghosh, A., J. E. Vidale, J. R. Sweet, K. C. Creager, and A. G. Wech (2009). Tremor patches in Cascadia revealed by seismic array analysis, *Geophys. Res. Lett.* **36,** L17316, doi: 10.1029/2009GL039080.

Ghosh, A., J. E. Vidale, J. R. Sweet, K. C. Creager, A. G. Wech, and H. Houston (2010). Tremor bands sweep Cascadia, *Geophys. Res. Lett.* **37,** L08301, doi: 10.1029/2009GL042301.

Goldstein, P., D. Dodge, M. Firpo, and L. Minner (2003). SAC2000: Signal processing and analysis tools for seismologists and engineers, *The IASPEI International Handbook of Earthquake and Engineering Seismology, Part B*, W. H. K. Lee, H. Kanamori, P. C. Jennings, and C. Kisslinger (Editors), Academic Press, London, United Kingdom.

Gomberg, J., J. L. Rubinstein, Z. Peng, K. C. Creager, J. E. Vidale, and P. Bodin (2008). Widespread triggering of nonvolcanic tremor in California, *Science* **319,** 173, doi: 10.1126/science.1149164.

Helffrich, G., J. Wookey, and I. Bastow (2013). *The Seismic Analysis Code: A Primer and User's Guide*, Cambridge University Press, New York, New York, 102–106.

Houston, H., B. G. Delbridge, A. G. Wech, and K. C. Creager (2011). Rapid tremor reversals in Cascadia generated by a weakened plate interface, *Nat. Geosci.* **4,** 404–409, doi: 10.1038/NGEO1157.

Huang, B.-S., C.-Y. Wang, D. Okaya, S.-J. Lee, Y.-C. Lai, F. T. Wu, W.-T. Liang, and W.-G. Huang (2013). Multiple diving waves and steep velocity gradients in the western Taiwan Coastal Plain: An investigation based on the TAIGER experiment, *Bull. Seismol. Soc. Am.* **103,** no. 2A, 925–935, doi: 10.1785/0120110047.

Idehara, K., S. Yabe, and S. Ide (2014). Regional and global variations in the temporal clustering of tectonic tremor activity, *Earth Planets Space* **66,** doi: 10.1186/1880-5981-66-66.

Kao, H., S. J. Shan, H. Dragert, G. Rogers, J. F. Cassidy, K. Wang, T. S. Jame, and K. Ramachandran (2006). Spatial-temporal patterns of seismic tremors in northern Cascadia, *J. Geophys. Res.* **111,** no. B3, doi: 10.1029/2005JB003727.

Kao, H., S. J. Shen, and K.-F. Ma (1998). Transition from oblique subduction to collision: Earthquakes in the southernmost Ryukyu arc-Taiwan region, *J. Geophys. Res.* **103,** no. B4, 7211–7229, doi: 10.1029/97JB03510.

La Rocca, M., D. Galluzzo, S. Malone, W. McCausland, G. Saccorotti, and E. Del Pezzo (2008). Testing small-aperture array analysis on well-located earthquakes, and application to the location of deep tremor, *Bull. Seismol. Soc. Am.* **98,** no. 2, 620–635, doi: 10.1785/0120060185.

Nadeau, R. M., and D. Dolenc (2005). Nonvolcanic tremors deep beneath the San Andreas fault, *Science* **307,** 389, doi: 10.1126/science.1107142.

Nadeau, R. M., and A. Guilhem (2009). Nonvolcanic tremor evolution and the San Simeon and Parkfield, California, earthquakes, *Science* **325,** 191–193, doi: 10.1126/science.1174155.

Nawab, S. H., F. U. Dowla, and R. T. Lacoss (1985). Direction determination of wideband signals, *IEEE Trans. Acoust. Speech Signal Process.* **33,** no. 5, 1114–1122, doi: 10.1109/TASSP.1985.1164705.

Nishizawa, A., K. Kameda, and M. Okawa (2009). Seismic structure of the northern end of the Ryukyu trench subduction zone, southeast of Kyushu, Japan, *Earth Planets Space* **61,** no. 8, e37–e40, doi: 10.1186/BF03352942.

Obara, K. (2002). Nonvolcanic deep tremor associated with subduction in southwest Japan, *Science* **296,** 1679–1681, doi: 10.1126/science.1070378.

Obara, K., and K. Chao (2013). Triggered tremor in inland region in Japan, *presented at 2013 Fall Meeting, AGU*, San Francisco, California, 9–13 December, Abstract S42B-04.

Peng, Z., and K. Chao (2008). Non-volcanic tremor beneath the Central Range in Taiwan triggered by the 2001 M_w 7.8 Kunlun earthquake, *Geophys. J. Int.* **175,** no. 2, 825–829, doi: 10.1111/j.1365-246X.2008.03886.x.

Peng, Z., and J. Gomberg (2010). An integrated perspective of the continuum between earthquakes and slow-slip phenomena, *Geophys. Res. Lett.* **3,** 599–607, doi: 10.1038/ngeo940.

Peng, Z., H. Gonzalez-Huizar, K. Chao, C. Aiken, B. Moreno, and G. Armstrong (2013). Tectonic tremor beneath Cuba triggered by the M_w 8.8 Maule and M_w 9.0 Tohoku-Oki earthquakes, *Bull. Seismol. Soc. Am.* **103,** no. 1, 595–600, doi: 10.1785/0120120253.

Peng, Z., J. E. Vidale, A. G. Wech, R. M. Nadeau, and K. C. Creager (2009). Remote triggering of tremor along the San Andreas fault in central California, *J. Geophys. Res.* **114,** no. B7, doi: 10.1029/2008JB006049.

Pollitz, F. F., R. Bürgmann, R. S. Stein, and V. Sevilgen (2014). The profound reach of the 11 April 2012 M 8.6 Indian Ocean earthquake: Short-term global triggering followed by a longer-term global shadow, *Bull. Seismol. Soc. Am.* **104,** no. 2, 972–984, doi: 10.1785/0120130078.

Pollitz, F. F., R. S. Stein, V. Sevilgen, and R. Bürgmann (2012). The 11 April 2012 east Indian Ocean earthquake triggered large aftershock worldwide, *Nature* **490,** 250–253, doi: 10.1038/nature11504.

Rogers, G., and H. Dragert (2003). Episodic tremor and slip on the Cascadia subduction zone: The chatter of silent slip, *Science* **300,** 1942–1943, doi: 10.1126/science.1084783.

Rost, S., and C. Thomas (2002). Array seismology: Methods and applications, *Rev. Geophys.* **40,** no. 3, 2-1–2-27, doi: 10.1029/2000RG000100.

Ryberg, T., C. H. Haberland, G. S. Fuis, W. L. Ellsworth, and D. R. Shelly (2010). Locating non-volcanic tremor along the San Andreas fault using a multiple array source imaging technique, *Geophys. J. Int.* **183,** no. 3, 1485–1500, doi: 10.1111/j.1365-246X.2010.04805.x.

Shelly, D. R. (2010). Migration tremors illuminate complex deformation beneath the seismogenic San Andreas fault, *Nature* **463,** 648–653, doi: 10.1038/nature08755.

Shelly, D. R., and J. L. Hardebeck (2010). Precise tremor source locations and amplitude variations along the lower-crustal central San Andreas fault, *Geophys. Res. Lett.* **37,** L14301, doi: 10.1029/2010GL043672.

Shelly, D. R., G. C. Beroza, and S. Ide (2007a). Non-volcanic tremor and low frequency earthquake swarms, *Nature* **446,** 305–307, doi: 10.1038/nature05666.

Shelly, D. R., G. C. Beroza, and S. Ide (2007b). Complex evolution of transient slip derived from precise tremor loctaions in western Shikoku, Japan, *Geochem. Geophys. Geosyst.* **8,** Q10014, doi: 10.1029/2007GC001640.

Shelly, D. R., W. L. Ellsworth, T. Ryberg, C. Haberland, G. S. Fuis, J. Murphy, R. M. Nadeau, and R. Bürgmann (2009). Precise location of San Andreas fault tremors near Cholame, California using seismometer clusters: Slip on the deep extension of the fault? *Geophys. Res. Lett.* **36,** L01303, doi: 10.1029/2008GL036367.

Shelly, D. R., Z. Peng, D. P. Hill, and A. Chastity (2011). Triggered creep as a possible mechanism for delayed dynamic triggering of tremor and earthquakes, *Nature Geosci.* **4,** 384–388, doi: 10.1038/ngeo1141.

Shin, T.-C., C.-H. Chang, H.-C. Pu, H.-W. Lin, and P.-L. Leu (2013). The geophysical database management system in Taiwan, *Terr. Atmos. Ocean. Sci.* **24,** no. 1, 11–18, doi: 10.3319/TAO.2012.09.20.01(T).

Tang, C.-C., Z. Peng, K. Chao, C.-H. Chen, and C.-H. Lin (2010). Detecting low-frequency earthquakes within non-volcanic tremor in southern Taiwan triggered by the 2005 M_w 8.6 Nias earthquake, *Geophys. Res. Lett.* **37,** no. 16, L16307, doi: 10.1029/2010GL043918.

Tang, C.-C., Z. Peng, C.-H. Lin, K. Chao, and C.-H. Chen (2013). Statistical properties of low-frequency earthquakes triggered by large earthquakes in southern Taiwan, *Earth Planet. Sci. Lett.* **373,** 1–7, doi: 10.1016/j.epsl.2013.04.039.

Tsai, Y.-B. (1986). Seismotectonics of Taiwan, *Tectonophysics* **125,** no. 1, 17–37, doi: 10.1016/0040-1951(86)90005-3.

Wech, A. G. (2010). Interactive tremor monitoring, *Seismol. Res. Lett.* **81,** no. 4, 664–669, doi: 10.1785/gssrl.81.4.664.

Wech, A. G., and K. C. Creager (2008). Automated detection and location of Cascadia tremor, *Geophys. Res. Lett.* **35,** L20302, doi: 10.1029/2008GL035458.

Wech, A. G., C. M. Boese, T. A. Stem, and J. Townend (2012). Tectonic tremor and deep slow slip on the Alpine fault, *Geophys. Res. Lett.* **39,** no. 10, doi: 10.1029/2012GL051751.

Wu, F. T., H. Kuo-Chen, and K. D. McIntosh (2014). Subsurface imaging, TAIGER experiments and tectonic models of Taiwan, *J. Asian Earth Sci.* **90,** 173–208, doi: 10.1016/j.jseaes.2014.03.024.

Wu, Y.-M., C.-H. Chang, L. Zhao, T.-L. Teng, and M. Nakamura (2008). A comprehensive relocation of earthquakes in Taiwan from 1991 to 2005, *Bull. Seismol. Soc. Am.* **98,** no. 3, 1471–1481, doi: 10.1785/0120070166.

Yao, D., Z. Peng, and X. Meng (2015). Remotely triggered earthquakes in South-Central Tibet following the 2004 M_w 9.1 Sumatra and 2005 M_w 8.6 Nias earthquakes, *Geophys. J. Int.* **201,** no. 2, 543–551, doi: 10.1093/gji/ggv037.

Yu, S., H.-Y. Chen, and L.-C. Kuo (1997). Velocity field of GPS stations in the Taiwan area, *Tectonophysics* **274,** 41–59, doi: 10.1016/S0040-1951(96)00297-1.

School of Earth and Atmospheric Sciences
Georgia Institute of Technology
311 Ferst Drive
Atlanta, Georgia 30332-0340
(W.-F.S., Z.P.)

Institute of Earth Sciences
Academia Sinica
128, Sec. 2, Academia Road
Nangang, Taipei 11529, Taiwan
(C.-H.L.)

Earthquake Research Institute
University of Tokyo
1-1-1 Yayoi, Bunkyo-ku
Tokyo 113-0032, Japan
(K.C.)

Manuscript received 27 August 2014;
Published Online 19 May 2015